Rapidity Dependence of Antiproton-to-Proton Ratios in Au + Au Collisions at $\sqrt{s_{NN}} = 130$ GeV

I. G. Bearden,[7] D. Beavis,[1] C. Besliu,[10] Y. Blyakhman,[6] J. Brzychczyk,[4] B. Budick,[6] H. Bøggild,[7] C. Chasman,[1] C. H. Christensen,[7] P. Christiansen,[7] J. Cibor,[3] R. Debbe,[1] J. J. Gaardhøje,[7] K. Grotowski,[4] K. Hagel,[8] O. Hansen,[7] A. Holm,[7] A. K. Holme,[12] H. Ito,[11] E. Jakobsen,[7] A. Jipa,[10] J. I. Jørdre,[9] F. Jundt,[2] C. E. Jørgensen,[7] T. Keutgen,[8] E. J. Kim,[5] T. Kozik,[4] T. M. Larsen,[12] J. H. Lee,[1] Y. K. Lee,[5] G. L. Løvhøiden,[12] Z. Majka,[4] A. Makeev,[8] B. McBreen,[1] M. Murray,[8] J. Natowitz,[8] B. S. Nielsen,[7] K. Olchanski,[1] J. Olness,[1] D. Ouerdane,[7] R. Płaneta,[4] F. Rami,[2] D. Röhrich,[9] B. H. Samset,[12] S. J. Sanders,[11] R. A. Sheetz,[1] Z. Sosin,[4] P. Staszel,[7] T. F. Thorsteinsen,[9,*] T. S. Tveter,[12] F. Videbæk,[1] R. Wada,[8] A. Wieloch,[4] and I. S. Zgura[10]

(BRAHMS Collaboration)

[1]*Brookhaven National Laboratory, Upton, New York 11973*
[2]*Institut de Recherches Subatomiques and Université Louis Pasteur, Strasbourg, France*
[3]*Institute of Nuclear Physics, Krakow, Poland*
[4]*Jagiellonian University, Krakow, Poland*
[5]*Johns Hopkins University, Baltimore, Maryland 21218*
[6]*New York University, New York, New York 10003*
[7]*Niels Bohr Institute, University of Copenhagen, Denmark*
[8]*Texas A&M University, College Station, Texas 77843*
[9]*University of Bergen, Department of Physics, Bergen, Norway*
[10]*University of Bucharest, Romania*
[11]*University of Kansas, Lawerence, Kansas 66045*
[12]*University of Oslo, Department of Physics, Oslo, Norway*

(Received 28 April 2001; published 24 August 2001)

Measurements, with the BRAHMS detector, of the antiproton-to-proton ratio at midrapidities and forward rapidities, are presented for Au + Au reactions at $\sqrt{s_{\rm NN}} = 130$ GeV, and for three different collision centralities. For collisions in the 0%–40% centrality range, we find $N(\bar{p})/N(p) = 0.64 \pm 0.04_{\rm (stat)} \pm 0.06_{\rm (syst)}$ at $y \approx 0$, $0.66 \pm 0.03 \pm 0.06$ at $y \approx 0.7$, and $0.41 \pm 0.04 \pm 0.06$ at $y \approx 2$. The ratios are found to be nearly independent of collision centrality and transverse momentum. The antiproton and proton rapidity densities vary differently with rapidity, and indicate a significant degree of collision transparency, although a net-baryon free midrapidity plateau (Bjorken limit) is not yet reached.

DOI: 10.1103/PhysRevLett.87.112305 PACS numbers: 25.75.–q

The reaction mechanism between heavy ions at high energies is expected to evolve from full stopping to complete transparency with increasing collision energy. In the case of full stopping, the baryons of the colliding nuclei will be shifted from the rapidity of the incident beam to midrapidity ($y \approx 0$), leading to the formation of a central zone with a significant excess in the number of baryons as compared to antibaryons (net-baryon density). In the case of full transparency, also called the Bjorken limit [1], the baryons from the interacting nuclei will, after the collision, also be shifted from the beam rapidity, but midrapidity will be devoid of original baryons. In this region, the net-baryon density is zero and the energy density is high. Almost complete stopping is observed for Au + Au reactions at AGS energies ($\sqrt{s_{NN}} \approx 5$ GeV). In reactions between lead nuclei at SPS energies ($\sqrt{s_{NN}} = 17$ GeV), transparency begins to set in, and systematics suggest that maximum baryon density occurs at energies intermediate between AGS and SPS (see, e.g., [2,3]). The situations of maximum baryon density and of vanishing net-baryon density at midrapidity give rise to entirely different initial conditions for the possible creation of a deconfined quark-gluon system.

The rapidity dependence of the antiproton to proton ratio in collisions between Au nuclei at the Relativistic Heavy Ion Collider (RHIC), Brookhaven National Laboratory, is investigated for $\sqrt{s_{NN}} = 130$ GeV, the highest center of mass energy yet achieved in collisions between heavy nuclei in the laboratory. The data were collected with the BRAHMS detector during the final two weeks of the first RHIC run, where the beam luminosity reached ≈10% of the nominal design value. We present measurements of the $N(\bar{p})/N(p)$ ratios at rapidities y(proton) ≈0, 0.7, and 2 as a function of collision centrality and transverse momentum together with $N(\pi^-)/N(\pi^+)$ ratios at $y(\pi) \approx 0, 1$, and 3. The measurements provide the first particle ratios over an extended rapidity range at RHIC energies and contribute to understanding the stopping mechanism at RHIC and the degree of transparency in the collisions. We find that, while the pion ratios are close to unity, the measured antiproton to proton ratio decreases from $0.64 \pm 0.04_{\rm (stat)} \pm 0.06_{\rm (syst)}$ at $y \approx 0$ and $0.66 \pm 0.03_{\rm (stat)} \pm 0.06_{\rm (syst)}$ at $y \approx 0.7$ to

$0.41 \pm 0.04_{(\mathrm{stat})} \pm 0.06_{(\mathrm{syst})}$ at $y \approx 2$ for 0%–40% collision centrality. The results show that a net-baryon-free midrapidity region has not been attained, although the $N(\bar{p})/N(p)$ ratio is the highest that has been measured thus far in nucleus-nucleus collisions. Recently, the STAR Collaboration has measured similar particle ratios at $y \approx 0$ in a narrower momentum range [4] and their results agree well with the $y \approx 0$ measurements presented here. The results as a function of rapidity are not consistent with model predictions.

The BRAHMS detector system [5] used in the present measurements consists of two independent magnetic spectrometers that can be positioned over an angular range from 2.3° to 30° (forward spectrometer, FS) and from 25° to 90° (midrapidity spectrometer, MRS) with respect to the beam line. A scintillator tile multiplicity array (TMA) measures charged particle emission in the central pseudorapidity region ($-2.0 < \eta < +2.0$) and is used for offline centrality selection. This detector consists of 38 square tiles of plastic scintillators ($12 \times 12 \times 0.5$ cm^3) forming a tube of hexagonal cross section with the axis along the beam pipe, such that no tile is placed in the MRS and FS acceptances. Two global detector systems cover forward angles. The zero degree calorimeters (ZDC) at ± 18 m from the nominal interaction point (IP) measure spectator neutrons [6]. The beam-beam bounters (BB) consist of two arrays with a total of 70 phototubes, each with a Cerenkov radiator, positioned ± 2.15 m, and measure charged hadrons in the pseudorapidity range of $3.0 < |\eta| < 3.8$. These two systems are used to define collision events by simultaneous measurements of the interaction vertex position.

For each actual vertex position, the total energy deposited in each ring of TMA tiles is determined. This energy loss signal is transformed to a charged particle multiplicity via division with the expected average energy deposited by one primary particle in a tile at its corresponding pseudorapidity. Centrality cuts are applied by selecting appropriate ranges in the multiplicity spectrum. The cuts can be expressed in terms of the fraction of the nuclear reaction cross section by normalization to the integral of the TMA spectrum obtained with a minimum bias trigger. This trigger requires energy deposition in each of the two ZDCs above 25 GeV with the additional condition of at least one tile having a hit. This requirement selects events corresponding to $\approx$99% $\pm$ 2% of the nuclear interaction cross section as deduced from simulations using HIJING. Centrality bins from 0% to 10%, 10% to 20%, and 20% to 40% of this event selection were used in the analysis.

In the present measurements, the MRS was operated at 90° and 40° and the FS at 4°, thus enabling the identification of protons and antiprotons in three rapidity intervals around $y = 0$, 0.7, and 2.0. The width of these intervals is less than 0.2 to 0.3 units of rapidity. The magnets of the two spectrometers were operated at fields allowing the reconstruction of particle tracks with laboratory momenta above $p \approx 0.2$ GeV/c in the MRS and above $p \approx 2$ GeV/c in the FS. The solid angles subtended by the MRS and FS are 6.5 and 0.8 msr, respectively. Each spectrometer consists of two time projection chambers (TPCs) positioned on either side of a dipole magnet and followed by a segmented scintillator time of flight (TOF) wall for particle identification (PID).

Particle momenta are determined by projecting the straight line tracks as reconstructed in the two TPCs to the magnet and calculating the momenta of matched tracks using an effective edge approximation. The momentum resolution is $\delta p/p \approx 0.01p$ for the FS, and for the MRS $\approx 0.04p(90°)$, and $\approx 0.03p(40°)$ at the field settings used. MRS tracks are required to originate from the primary vertex as determined by the BB counters within ± 5 cm horizontally, and ± 2.5 cm vertically from the nominal beam position. Tracks in the FS have looser horizontal matching requirement (± 12 cm) and vertical (± 5 cm) cuts due to the uncertainty from projecting tracks back to the beam line. PID requires not only a TOF measurement, but also the determination of the flight distance and thus of the collision vertex position on an event by event basis. The BB counters have an intrinsic time resolution of 65 ps and permit a determination of the collision vertex position to $\approx \pm 2$ cm by measuring the difference in arrival time of particles in the two arrays. This method is confirmed by projecting tracks determined in the first TPC of the MRS back to the beam plane. The collision vertex distribution was approximately of Gaussian shape with $\sigma \approx 70$ cm. Events with vertices between ± 15 cm for MRS and ± 40 cm for FS, respectively, are selected. The two TOF arrays are positioned at 4.3 m (MRS) and 8.6 m (FS) from the IP, respectively. The overall time resolution was determined to be $\sigma(\mathrm{TOF}) \approx 120$ ps.

Kaons and protons are separated in the momentum range $p < 2.4$ GeV/c and $p < 4.5$ GeV/c in the MRS and FS, respectively. Kaons and pions can be separated up to $p = 1.6$ GeV/c in MRS. In the FS at the 4 degree setting, kaons could not be cleanly separated from pions, although the $N(\pi^-)/N(\pi^+)$ ratio for $0.15 < p_t < 0.3$ GeV/c could be determined with only a small kaon contamination. Figure 1 demonstrates the PID achieved in the MRS and FS, respectively. The lower two panels show the m^2 spectra obtained for positively charged particles (π^+, K^+, p) and the upper two panels for negative particles ($\pi^-, K^-, \bar{p}$). These distributions were calculated using the particle momentum, TOF, and flight distance. The MRS data shown are from $0.4 < p_t < 2.4$ GeV/c, while the FS data are from $0.15 < p_t < 0.55$ GeV/c.

The particle yield in the FS is determined by selecting tracks having a TOF within a $\pm 2\sigma$ band of the expected TOF vs momentum for a given particle type. The results of such cuts for pions and protons are shown in Fig. 1. In the MRS, where the momenta are much lower and the particle peaks better separated, the yields are determined by applying cuts in the m^2 spectra, as seen in Fig. 1. The number of particles measured at either polarity is normalized to the number of collision events defined by the BB-ZDC

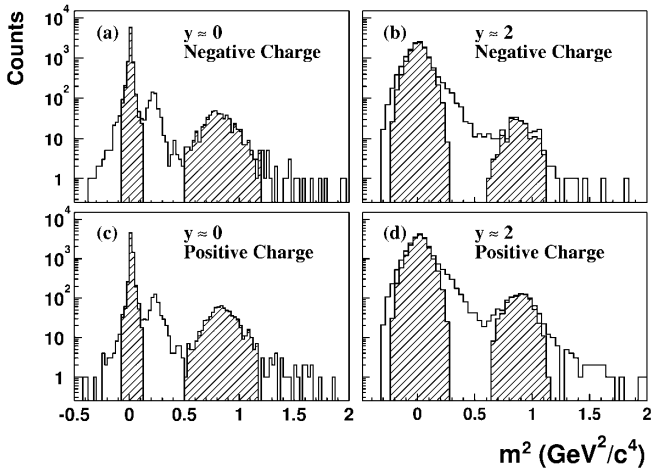

FIG. 1. Distributions of m^2 for charged particles identified in the BRAHMS spectrometers. The left panels (a) and (c) show data from the MRS at 90° for negatively and positively charged particles, respectively. The hatched areas show the pions selected for analysis in the momentum range $p < 1.6$ GeV/c and $-0.075 < m^2 < 0.125$, and the protons for $p < 2.4$ GeV/c and $0.5 < m^2 < 1.2$. The right panels (b) and (d) show data from the FS at 4°. The hatched region for these panels shows a yield of particles selected for analysis on the basis of fiducial cuts on time of flight for a momentum range of $2 < p < 4$ GeV/c.

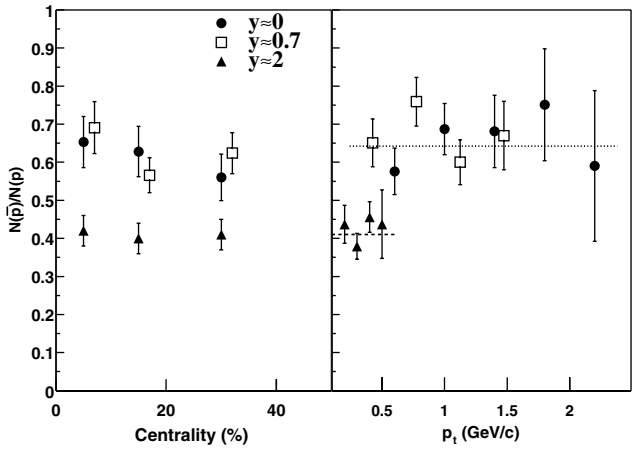

FIG. 2. The left panel shows the centrality dependence of the $N(\bar{p})/N(p)$ ratios for the three rapidity values: $y \approx 0$ (filled circles, MRS), $y \approx 0.7$ (open squares, MRS), and $y \approx 2$ (filled triangles, FS). Only statistical errors are shown. The data points for $y \approx 0.7$ are shifted slightly for display purposes. The centrality percentages are described in the text. The right panel shows the transverse momentum dependence of the measured $N(\bar{p})/N(p)$ ratio for the same three rapidity intervals for events selected from the 0%–40% centrality cut. The upper dotted line shows the average ratio for $y \approx 0$, while the dashed line for $y \approx 2$.

coincidences fulfilling a given centrality cut described above and the ratios are calculated.

The acceptances for the spectrometers for positively charged particles at one field are equal to the acceptances for negatively charge particles at the opposite polarity. Thus, in ratios of numbers of particles, measured at opposite field polarities, most systematic errors cancel out. The ratios have been corrected for losses of antiprotons due to annihilation as evaluated by GEANT simulations. The corrections are less than 2% in the MRS and about 3.5% in the FS. It is noted that backgrounds from misidentified tracks and from the tails of kaon and pion peaks are small and affect the extracted ratios negligibly (<1%). In the MRS, the background contribution from slow protons, arising mainly from the interaction of pions with the Be beam pipe, is ≈10% for the lowest p_t bin. The data have been corrected for this effect. In the FS, this contribution is found to be negligible. The systematic uncertainty in the particle ratios is estimated to ±10%. The dominant source of uncertainty is the normalization to the number of reactions (≈5%). The remaining systematic uncertainty is due to several smaller sources (each <1%), e.g., corrections for the background of slow protons, corrections for antiproton absorption, and errors associated with the tracking and PID and the vertex determination.

Figure 2 shows the dependence of the measured $N(\bar{p})/N(\bar{p})$ ratios on collision centrality and on particle transverse momentum. Figure 2(a) shows the centrality dependence for data summed over all momentum bins, while Fig. 2(b) shows the p_t dependence for data summed over all centrality bins. It is seen that the centrality dependence of the ratio is small for the three considered rapidities. The $N(\pi^-)/N(\pi^+)$ ratios (not shown) exhibit a similar lack of centrality and p_t dependence.

The ratios shown in Fig. 2 have not been corrected for protons and antiprotons that originate from weak decays of hyperons (Λ, Σ, etc.). We have studied the magnitude of the corrections in our acceptance using various assumptions as input to GEANT simulations. Assuming primary hyperon to baryon $[N(H)/N(B)]$ ratios of up to 0.5, we find that the correction to the quoted ratios is less than ±5% for $N(\bar{H})/N(H)$ between 0.4 and 0.8 ($y \approx 0$) and between 0.3 and 0.5 ($y \approx 2$).

In Figure 3, we summarize the rapidity dependence of the measured particle ratios calculated for the 0%–40% most central collisions. The upper and lower panel depict the $N(\pi^-)/N(\pi^+)$ and $N(\bar{p})/N(p)$ ratios, respectively. It is seen that, while the pion ratio is independent of rapidity and consistent with unity, the antiproton to proton ratio drops significantly with increasing rapidity.

The $N(\bar{p})/N(p)$ ratio of 0.64 found here at $y \approx 0$ is considerably higher than the similar ratios measured in Pb + Pb collisions at the SPS (≈0.07–0.15 at $\sqrt{s_{NN}} = 17$ GeV) [7,8] and at the AGS (≈2.5×10^{-4} at $\sqrt{s_{NN}} = 5$ GeV) [9]. It is, in fact, close to the $p + p$ result (0.61 ± 0.10) [10] at $\sqrt{s_{NN}} = 63$ GeV and $p_t \approx 0.3$ GeV/c, and below the value obtained by an extrapolation of the $p + p$ data from this reference to 130 GeV center of mass (c.m.) energy. The rapidity dependence of the ratios, which are unique to the present measurement, is of particular interest for the understanding of the reaction dynamics. The $N(\bar{p})/N(p)$ at $y \approx 0$ and ≈0.7 are approximately the same, consistent with the formation of a plateau around midrapidity. The decrease

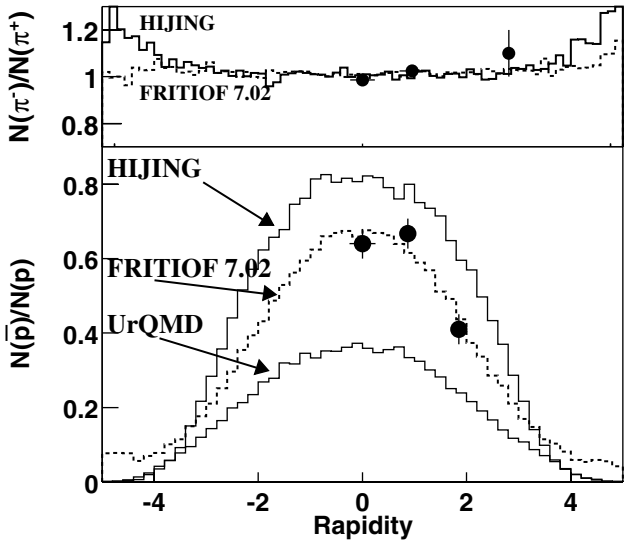

FIG. 3. Comparison of the measured $N(\bar{p})/N(p)$ (lower panel) and $N(\pi^-)/N(\pi^+)$ (upper panel) ratios to model predictions. The data shown are for 0%–40% central events and integrated over the transverse momentum range shown in Fig. 2. The three model calculations (HIJING, FRITIOF, and UrQMD) are shown for comparison. See text for details.

in the ratio over the next unit of rapidity is larger than observed in $A + A$ collisions at lower energies, but is very similar to the $p + p$ result at roughly half the c.m. energy [11]. The observed magnitude of the antiproton to proton ratio at $y \approx 0$ and 0.7 suggests that in the measured collisions a high degree of transparency is obtained leading to a region with low net-baryon density around midrapidity covering at least ± 1 units of rapidity. The $y = 2$ result of a significantly smaller antiproton to proton ratio shows that the net baryon poor plateau does not extend to $y = 2$, an observation that provides a severe test for theoretical model descriptions of the collision mechanism.

In Fig. 3, we compare the measured ratios to calculations using the HIJING model [12], the FRITIOF 7.02 string model [13], and the UrQMD cascade model [14] using the same centrality cuts as in the data analysis. Hyperon decays have not been included in the calculations shown, but affect the results by less than 5%. All three models reproduce the observed pion ratios well. FRITIOF reproduces our $N(\bar{p})/N(p)$ ratios, while overpredicting (by $\approx$30%) the charged particle yield at $\eta \approx 0$ [15]. This is due to a significant degree of stopping in the model. On the other hand, HIJING, which describes the overall charged particle yields at $\eta \approx 0$, fails in describing the antiproton to proton ratio. This feature of the model is related to the small stopping of the projectile baryons. The UrQMD model, which is not a partonic model, underpredicts the ratio by nearly a factor of 2. None of the models offer a consistent description of the observed features in this energy regime.

In summary, the BRAHMS experiment has measured the ratio of positive and negative pions and protons at midrapidities and forward rapidities. We find that the pion ratios are close to unity as would be expected at these energies. We find, however, that for central collisions at $\sqrt{s_{NN}} = 130$ GeV the ratio of antiprotons to protons is still significantly below unity at midrapidity and decreases towards forward rapidity. In addition, the reactions at the present energy evidence the highest antiparticle/particle ratios thus far observed in energetic nucleus-nucleus collisions. The rapidity dependence serves as an indicator of baryon number transport to the central region. Although there is evidence for transparency in the reaction and the onset of the decoupling of the net-baryon rich fragmentation region from the net-baryon poor central region, the present result demonstrates that there is still a significant contribution from participant baryons over the entire rapidity range.

The BRAHMS Collaboration wishes to thank the RHIC team for their support. This work was supported by the Division of Nuclear Physics of the Office of Science of the U.S. Department of Energy, the Danish Natural Science Research Council, the Research Council of Norway, the Jagiellonian University Grant, the Korea Research Foundation Grant, and the Romanian Ministry of Education and Research.

*Deceased.

[1] J. D. Bjorken, Phys. Rev. D **27**, 140 (1983).
[2] N. Herrmann, J. P. Wessels, and T. Wienold, Annu. Rev. Nucl. Part. Sci. **49**, 581 (1999).
[3] F. Videbæk and O. Hansen, Phys. Rev. C **52**, 2684 (1995).
[4] STAR Collaboration, C. Adler *et al.,* Phys. Rev. Lett. **86**, 4778 (2001).
[5] D. Beavis *et al.,* Conceptual Design Report for BRAHMS, BNL-62018; BRAHMS Collaboration, I. G. Bearden *et al.* (to be published).
[6] C. Adler *et al.,* Nucl. Instrum. Methods (to be published); /xxx.lanl.gov/nucl-ex/0008005.
[7] NA44 Collaboration, I. G. Bearden *et al.,* J. Phys. G, Nucl. Part. **23**, 1865 (1997); M. Kaneta, Ph.D. thesis, University of Hiroshima, 1998.
[8] NA49 Collaboration, F. Sickler *et al.,* Nucl. Phys. **A661**, 45c (1999); G. E. Cooper, Ph.D. thesis, University of California–Berkeley, 2000.
[9] E802 Collaboration, L. Ahle *et al.,* Phys. Rev. Lett. **81**, 2650 (1998).
[10] K. Guettler *et al.,* Nucl. Phys. **B116**, 77 (1976).
[11] P. Capiluppi *et al.,* Nucl. Phys. **B79**, 189 (1974).
[12] HIJING 1.36 with Parton shadowing and Jet quenching. X.-N. Wang and M. Gyulassy, Phys. Rev. D **44**, 3501 (1991).
[13] B. Anderson *et al.,* Z. Phys. C 485 (1993); H. Pi, Comput. Phys. Commun. **71**, 173 (1992).
[14] S. A. Bass *et al.,* Prog. Part. Nucl. Phys. **41**, 225 (1998); M. Bleicher *et al.,* J. Phys. G, Nucl. Part. **25**, 1859 (1999).
[15] B. Back *et al.,* Phys. Rev. Lett. **85**, 3100 (2000).